Heavy Ion Elastic Recoil Detection Analysis of Optoelectronic and Semiconductor Devices

N. Dytlewski and D. Cohen (1), H. Whitlow and M. Hult (2), M. Ostling and C. Zaring (3), P. Johnston and S. Walker (4)

(1) Australian Nuclear Science and Technology Organisation,Lucas Heights
(2) University of Lund, Sweden
(3) Royal Institute of Technology, Stockholm, Sweden
(4) Royal Melbourne Institute of Technology, Australia

Abstract

ERDA time of flight spectrometry gives simultaneously, mass resolved elemental concentration profiles of complex structures. A major advantage of this technique, is the ability to see light elements in a heavy matrix. This technique has been applied to measure the diffusion , stoichiometry and light element distributions in devices during the manufacture of semiconductor devices used for optoelectronics, telecommunications and solar power generation.
A beam of 77 MeV I^{10+} produced by the ANTARES Tandem accelerator, generated target recoil atoms which were detected in a time of flight plus total energy detector spectrometer positioned at 45° to the incident beam, with the data recorded by a multiparameter data acquisition system using VME electronics and DEC 5000 Risc workstations. Some applications to be described include the device structure Si/SiO2/poly-Si/W which resembles a MOS gate with the tungsten as a conducting overlayer. The tungsten is deposited by the LPCVD-W process, and the objective is to study the behaviour and amount of fluorine upon heat treatment, which accumulates at the oxide interfaces. In another application, a thin film solar cell with structure soda-lime glass/Mo/CuInSe2 is investigated to study the diffusion of sodium from the glass substrate into the active surface layer.

Introduction

In recent years, the use of heavy ion mass and energy dispersive time-of-flight elastic recoil spectrometry (HIERDA) has been applied to analyse multi-phase, thin layer devices used in optoelectronics, semiconductors and solar power generation. HIERDA gives simultaneously, mass resolved elemental depth distributions which are free of the matrix and sputtering induced artifacts that limit Auger profiling and SIMS. HIERDA is similar to RBS, but has the difference that the recoiling target atoms are detected instead of the scattered projectile. High energy, heavy ions beams (typically 50MeV - 100MeV ^{127}I) bombard the sample, ejecting recoil atoms which are detected at a forward angle, typically 45°. A time-of-flight and total energy detection system enables the ejected particle's mass to be identified, and allows energy spectra to be obtained and interpreted in an analogous way to RBS, but with the important difference that the elemental spectra are separated, and not superimposed on a background as in RBS. This effect makes for good sensitivity, the analysis of light element distributions in a heavy matrix. In this paper, we describe some of the measurements made with a HIERDA system on the ANTARES Tandem Accelerator at ANSTO.

Experimental

A heavy ion beam of ^{127}I was injected into the Tandem Accelerator with terminal voltage set at 7MV, with the emergent 77 MeV 10+ charge state directed into the experimental target chamber. Beam stripping was with a 3 μg/cm2 carbon foil. The 10+ charge state was selected as it gave sufficient target current; the yield of the 11+ charge state is approx. 50% that of the 10+ state, while the 12+ state is only approx. 10% . Iodine is chosen as the projectile species as the ERDA cross-section varies as Z^2 , and as the t-o-f detector is positioned at 45°, it is kinematically not possible for the iodine beam to be scattered off elements with mass < 90, and enter the detector. Also, as iodine is mono-

isotopic, good beam transmission can be achieved from the ion source to the target chamber. The major problem in producing high energy beams of iodine, is the lifetime of the carbon stripper foil; typically 2 to 3 hrs for 50nA of I^- injected beam into the Tandem Accelerator. When a new carbon stripper foil is inserted into the stripper canal, the output iodine beam current initially rises rapidly, then slowly decreases with an approx. half-life of 2 hrs. The target current is maintained by increasing the injected iodine beam but eventally, a new stripper foil is required. In a typical measurement day of 16 hrs, 5 stripper foils are used. After the iodine beam is energy analysed by a 90° analyser magnet, it enters a switching magnet, where is is deflected 27° into the IBA beamline and target chamber. The vacuum system of the Tandem Accelerator and target chamber is maintained at a vacuum of typically 10^{-5} Pa by cryopumps.

The target positioning and time-of-flight detector system is shown in fig. 1. A small defining aperture inside the target chamber restricts the beamspot size on the target to 5x3 mm. The target is inclined at 30° to the iodine beam, with the time-of-flight detector positioned at 45°. The t-o-f detector was brought to Australia from Sweden by Harry Whitlow and Mikael Hult, and installed on the Australian target chamber. The t-o-f detector is the electrostatic mirror type, as developed by Busch /1/. When a recoil target atom passes through a thin carbon foil, the backward emitted secondary electrons are bent through 90° and collected by a pair of stacked microchannel plates. The output pulse is input to a fast constant fraction discriminator, which feeds one input of a triple coincidence unit. Three coincidences are required to flag a valid recoil atom; two pulses from the t-o-f detector (start & stop flight time), and a third from the total energy, ion-implanted detector. Triple coincidence rates were typically 20Hz - 40Hz, with unsuppressed target currents of approx. 20 charge nA. The analog energy and t-o-f pulses are collected by VME -ADC's, triggered by the triple coincidence, with the digitised data transferred via ethernet to DEC5000 RISC workstations, where two-dimensional, on-line graphical displays are produced. Off-line graphics production and analysis is via the CERN Physics Analysis Workstation software PAW.

Measurements

The focus of the measurements made to date have been metallisation studies on substrate materials from columns III and V in the periodic table, investigating the formation of various ohmic contacts to AlGaAs, GaAs, InP and related materials for use in two-dimensional electron devices. The contact resistance and device performance depends strongly on the interaction of the contact material with the active device layers, and it is of interest to follow certain aspects of the manufacturing technology. Rather than presenting a detailed interpretation of the data obtained, a qualitative overview will be given, with reference to three structures, which outline some of the capabilities of the HIERDA technique. It should be noted that in the accompanying figures, the mass calibration scale is only preliminary, and hence mass-energy (channel) curves can appear a few mass positions away from the expected value. However, from a knowledge of the structure, one can easily associate a mass curve with an element of the periodic table.

Sample #1 $Si/CoSi_2/Si/a\text{-}Si/B/a\text{-}Si$

A contact layer of interest is $CoSi_2$. The di-silicide stoichiometric mix is the most conducting phase, with a reported resistivity of approx. 13 micro-ohm cm. It has also a rather high temperature stability, which should make it a suitable contact structure. Of interest, is the diffusion of some ion implant species, in this case boron, into the contact layer. The following structure was analysed:

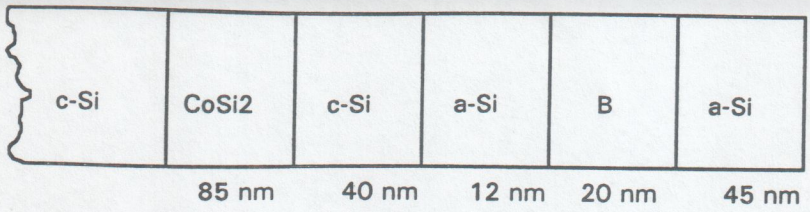

The objective is to study the boron distribution, and subsequent solubility of boron in $CoSi_2$ upon heat treatment. The $CoSi_2$ was formed by ion implantation of Co into Si, and heat treated to form epitaxial silicide. Boron and silicon was then electron beam evaporated on top to form the layered structure, then heat treated at 900° C for 24hrs. Fig. 2 shows the HIERDA spectra of this sample. In the mass vs energy diagram, the strong continuous silicon mass-energy and weaker boron curves are seen. There is also the presence of oxygen and titanium, which results from stray iodine beam hitting part of a titanium backing plate on which the samples were mounted. In the ADC1 vs ADC2 diagram, the short curve corresponding to cobalt recoils is seen, as is another short track corresponding to multiply scattered iodine beam entering the detector. In fig.3, a two-dimensional surface plot is presented which more graphically illustrates the boron and oxygen yields as a function of depth. It remains to transform the measured yield information into a quantitative concentration-depth distribution.

Sample #2 $Si/SiO_2/poly\text{-}Si/CoSi_2$ implanted with BF_2^+ (75 keV, dose $10^{15}/cm^2$)

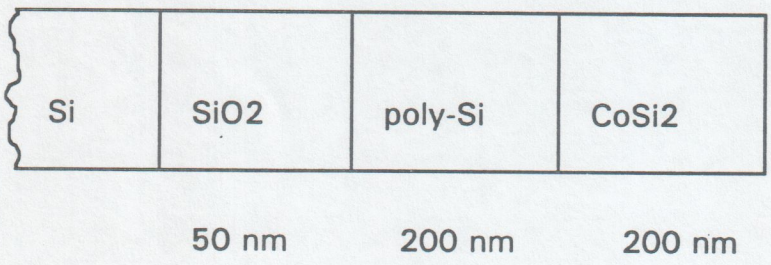

In this sample, boron was reportedly implanted in a molecular form, and the objective was to study the fluorine redistribution upon heat treatment of this MOS gate structure. The fluorine is expected to concentrate at the oxide interfaces. Four samples were implanted and measured; as implanted, and annealing temperatures of 650°C, 850° C and 1050°C for 1 hr. In fig. 4, a surface view of the silicon yield is shown, and in the "as implanted" view, it can be seen that near the surface, the silicon yield is low (CoSi layer), then increases sharply (poly-Si layer), decreases again (SiO_2 layer), then rises again (Si substrate). Heating to 650°C shows no change, but at 850°C, there is an increase in silicon yield for this surface layer, with a corresponding decreased yield from the second layer. This is due to cobalt diffusing from the first layer into the second, as is seen by the width of the cobalt yield in fig. 5. The buried oxygen layer and boron implant is easily seen in fig. 6, which is an expanded view of the un-annealed sample. Also evident, is some surface oxygen contamination. What is suprising, and is observed in all 4 samples, is that there is no evidence of any fluorine. The mass calibration is reasonably good for this sample in the low mass region, so that we cannot ascribe the "surface oxygen" peak as the fluorine implant. As the author (ND) has no knowledge on how this sample was prepared, one must assume that the reported method of boron implant was incorrect.

Also of interest, is the change in the buried oxide layer. In fig. 7, a projection of the oxygen yield onto the energy (channel) axis is presented for the 4 samples measured, the solid curve is the "as implanted" sample. The yield curves for the "as implanted" and 650° C samples are coincident, but for the higher temperature annealed samples, a spectrum shift to higher energies, and width broadening is observed. This is indicative of a small, but measurable, redistribution of the oxygen. This is more obvious in fig. 8, which shows a comparison between the "as implanted" and 1050°C sample.

Sample #3 Solar Cell soda-lime glass/Mo/$CuInSe_2$

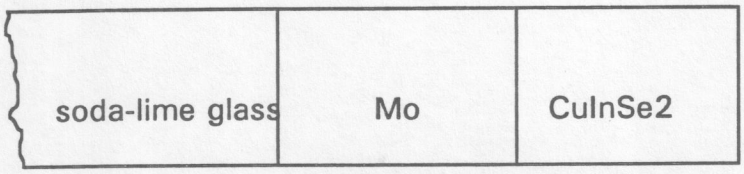

1000 nm 2500 nm

In this type of thin solar cell based on a soda-lime glass substrate, the active layer is $CuInSe_2$. Of interest, is the diffusion of sodium from the glass substrate into the active layer upon heat treatment. The properties of the active layer depends on the impurtity types and concentrations. This case is also of interest as it demonstrates the profiling by HIERDA of a light element in a thick, heavy matrix Mo. Two samples were prepared without the active surface layer present, to study the diffusion of sodium through the molybdenum. In fig. 9, the "as deposited" view shows no initial sodium content as expected, but some carbon, nitrogen and oxygen contamination is present. Another prepared sample heated to 550°C for 1 hr, shows in fig. 9 the presence of the diffused sodium and possibly also, a low level of silicon. This sample has also more carbon and oxygen contamination.

Summary

The data presented in this paper represents some of the results of a joint project in HIERDA between Sweden and Australia; the time-of-flight detector provided by Sweden, and the Tandem Accelerator and multi-parameter data acquisition facilities provided by Australia.

From the described measurements, it is apparent that HIERDA offers the capability to investigate complex structures and processes in today's high technology areas. The good mass resolution for the light elements, and the ability to do depth profile studies in the presence of a heavy matrix, will, with

RBS and hydrogen specific ERDA, will open the way for previously thought difficult R&D projects, because of the number of separate analytical tools required to provide the necessary data. Much work still remains to fully optimise HIERDA systems for mass and depth resolution. Of immediate need, is computer software to convert the measured mass yield profiles into concentration vs depth profiles. The algorithms for this process are similar to that for the RBS program RUMP, but are a more complex extension. The challenge is to fully exploit this measurement technology.

References

/1/F. Busch, W. Pfeffer, B. Kohlmeyer, D. Schull and F. Puhlhoffer, Nucl. Inst. Meth. 171(1980)71.

Figure captions

Fig. 1 Schematic diagram of experimental setup.

Fig. 2 Energy and timing spectra for sample #1, and the 2-dimensional mass-energy transformations.

Fig. 3 Surface contour plot of the oxygen and boron yields for sample #1.

Fig. 4 Surface contour plots of the silicon yields at different temperatures, for sample #2.

Fig. 5 Cobalt yields for different temperatures, for sample #2.

Fig. 6 Magnified surface yield plots for sample #2, showing a large oxygen yield from the buried layer, surface oxygen contamination, and a small peak due to the implanted boron.

Fig. 7 Oxygen yield vs channel (depth) for 4 different processing temperatures. The solid curve is the "as implanted" sample.

Fig. 8 Comparison between the oxygen yield curves for the "as implanted" sample (solid curve), and the 1050°C sample (dashed curve).

Fig. 9 Surface plot of sample #3, showing in the upper view, no sodium, but when heated to 550°C, some sodium diffusion in the molybdenum is seen.

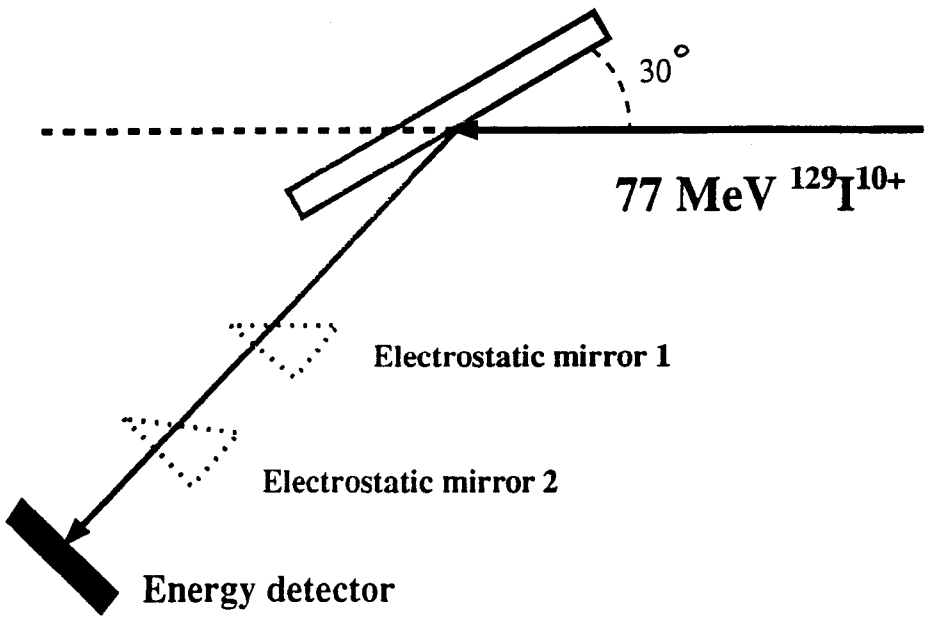
30°
77 MeV $^{129}I^{10+}$
Electrostatic mirror 1
Electrostatic mirror 2
Energy detector

Figure. 1

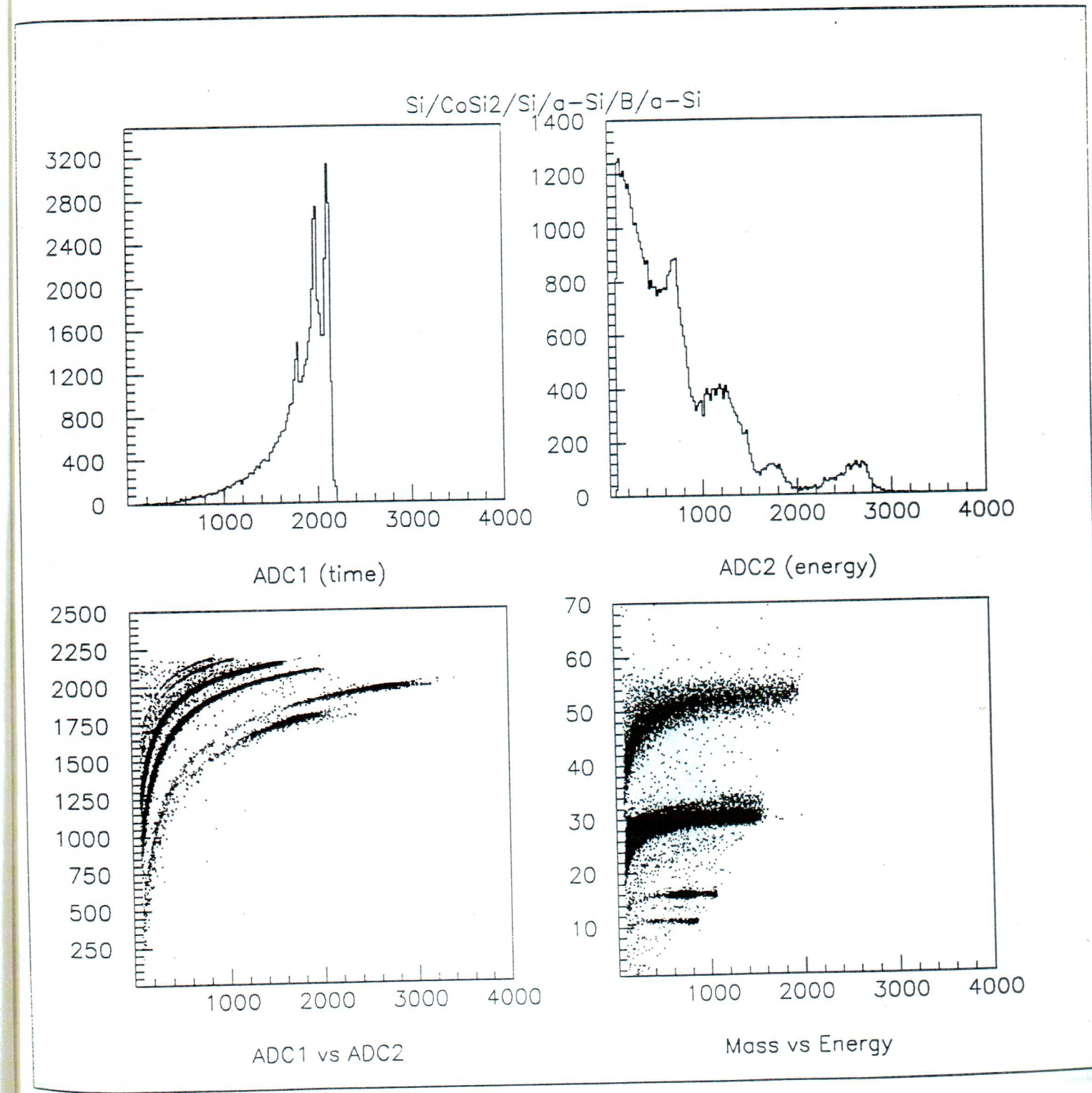
Si/CoSi2/Si/a-Si/B/a-Si
3200
2800
2400
2000
1600
1200
800
400
0
1000
2000
3000
4000
ADC1 (time)
1400
1200
1000
800
600
400
200
0
1000
2000
3000
4000
ADC2 (energy)
2500
2250
2000
1750
1500
1250
1000
750
500
250
1000
2000
3000
4000
ADC1 vs ADC2
70
60
50
40
30
20
10
1000
2000
3000
4000
Mass vs Energy

Figure 2

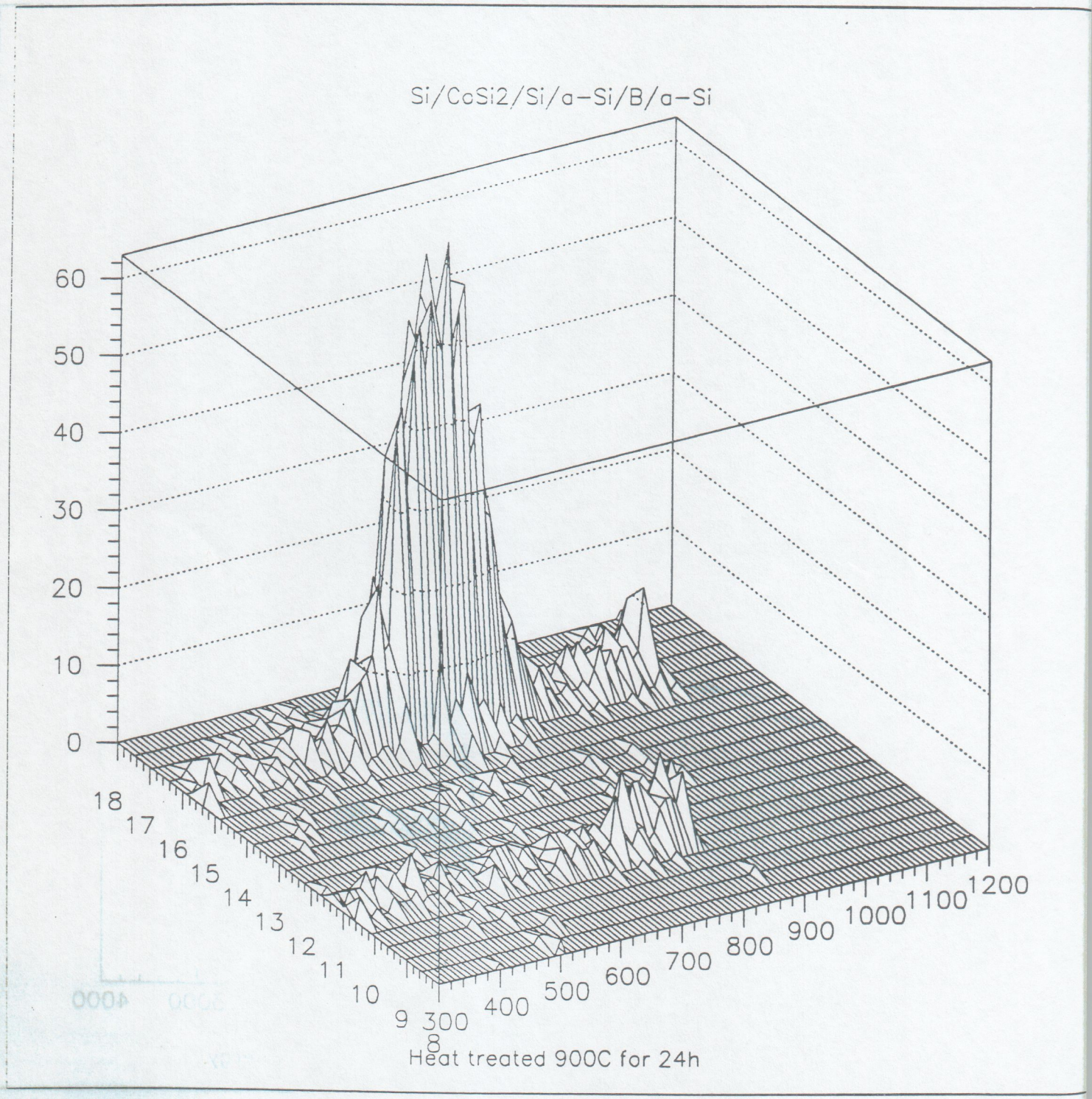
Si/CoSi2/Si/a-Si/B/a-Si
60
50
40
30
20
10
0
18
17
16
15
14
13
12
11
10
9
8
300
400
500
600
700
800
900
1000
1100
1200
Heat treated 900C for 24h

Figure 3

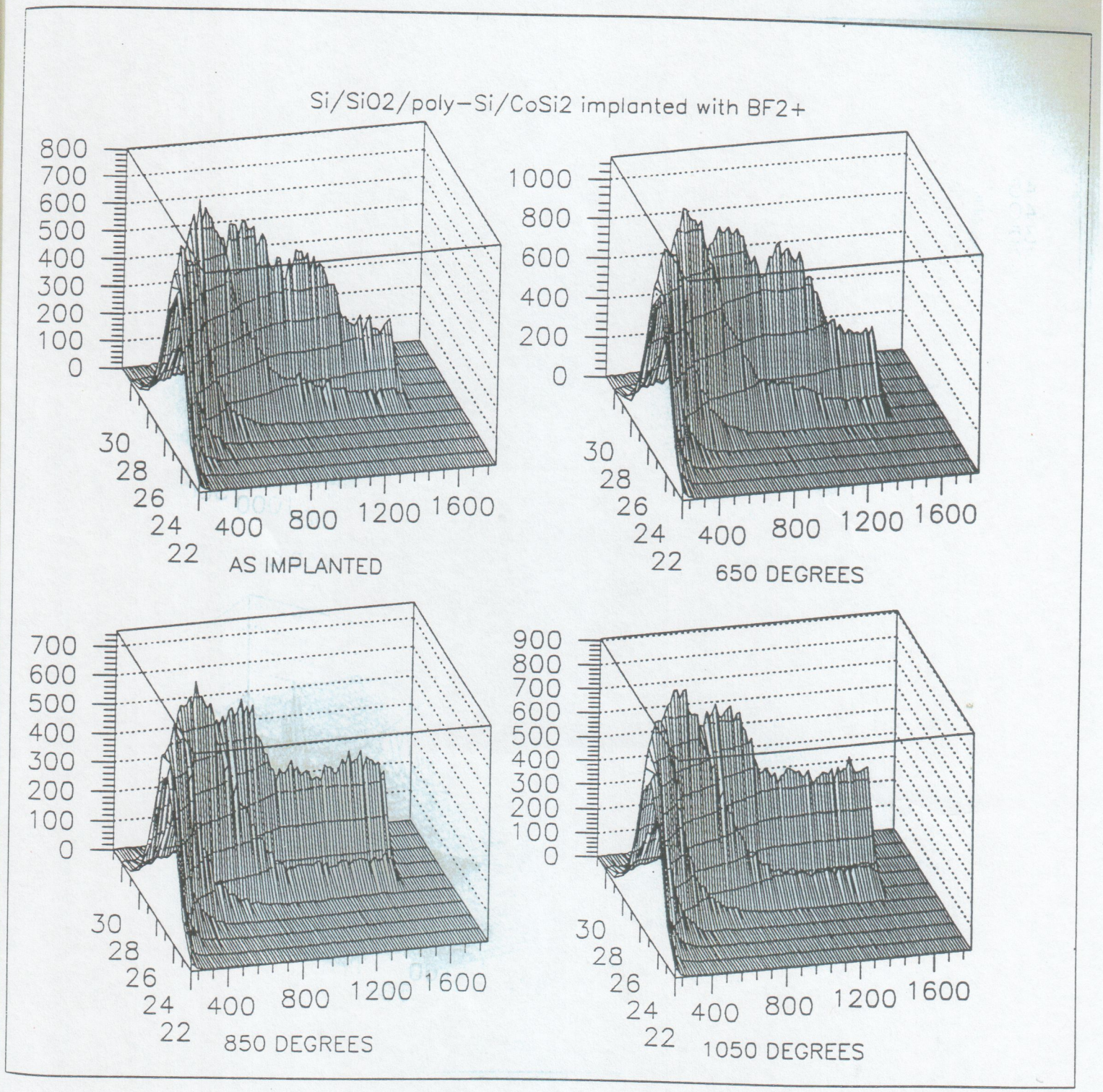
Si/SiO2/poly–Si/CoSi2 implanted with BF2+
AS IMPLANTED
650 DEGREES
850 DEGREES
1050 DEGREES

Figure 4

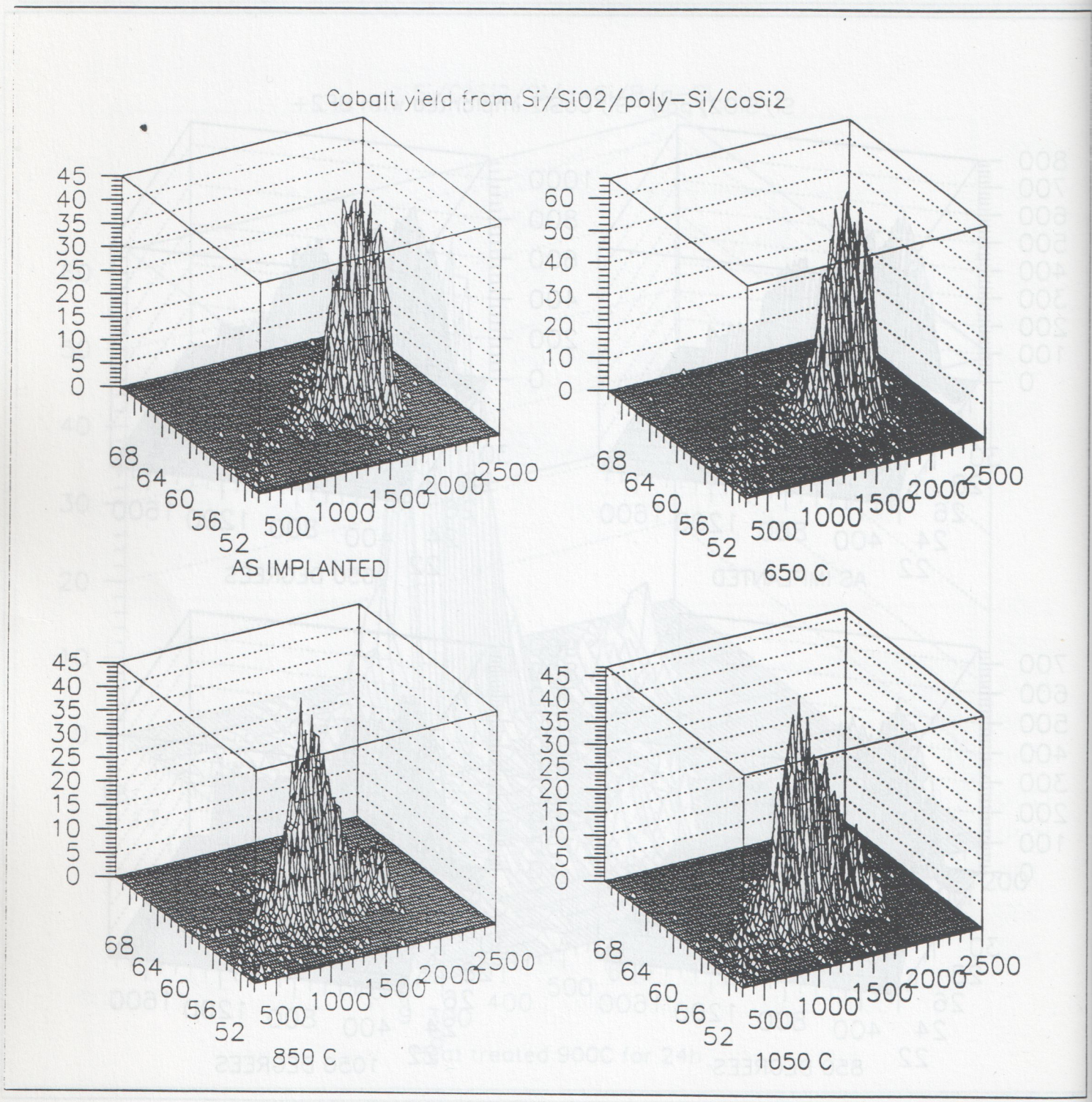
Cobalt yield from Si/SiO2/poly-Si/CoSi2
AS IMPLANTED
650 C
850 C
1050 C

Figure 5

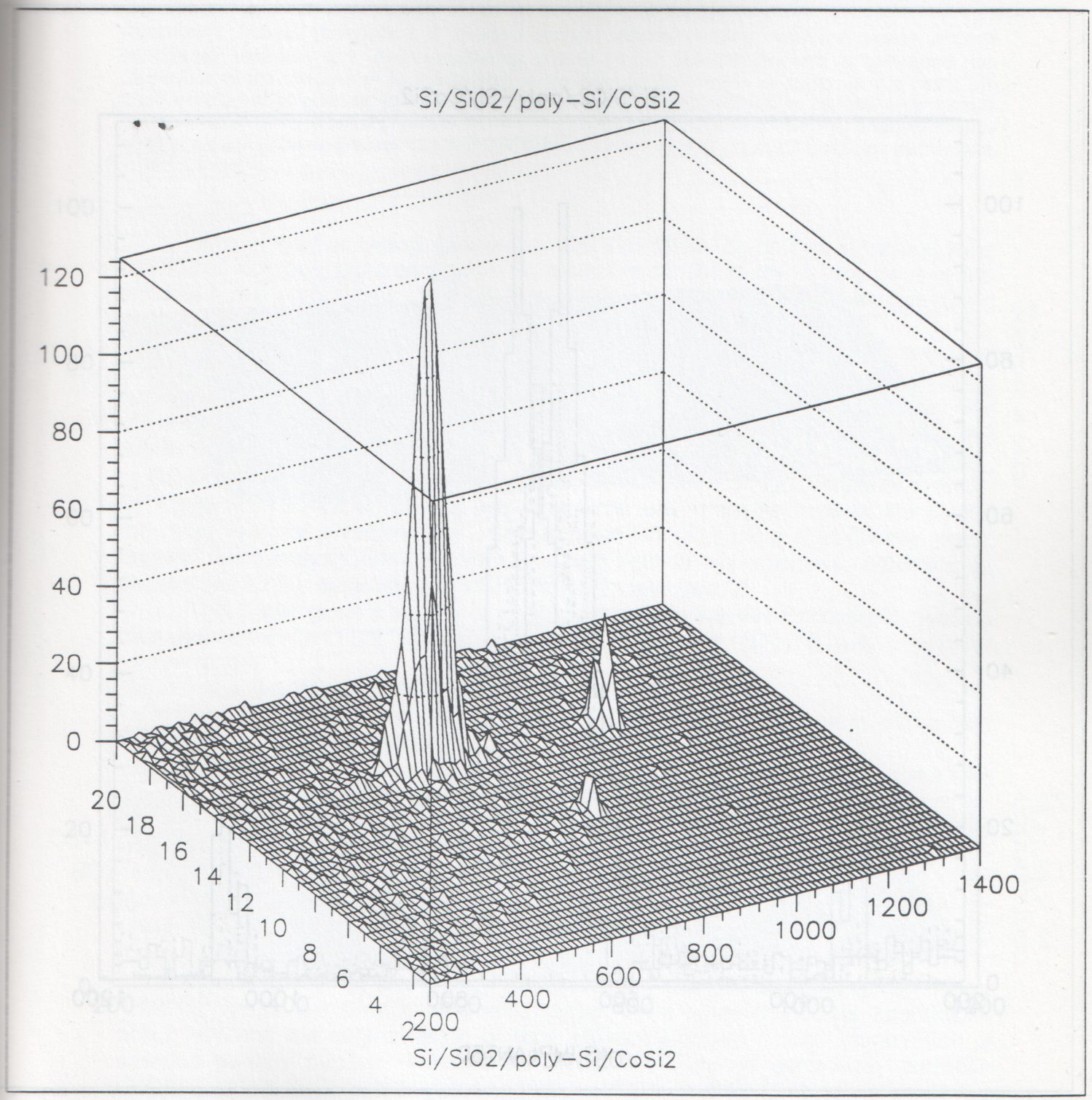
Si/SiO2/poly-Si/CoSi2
120
100
80
60
40
20
0
20
18
16
14
12
10
8
6
4
2
200
400
600
800
1000
1200
1400
Si/SiO2/poly-Si/CoSi2

Figure 6

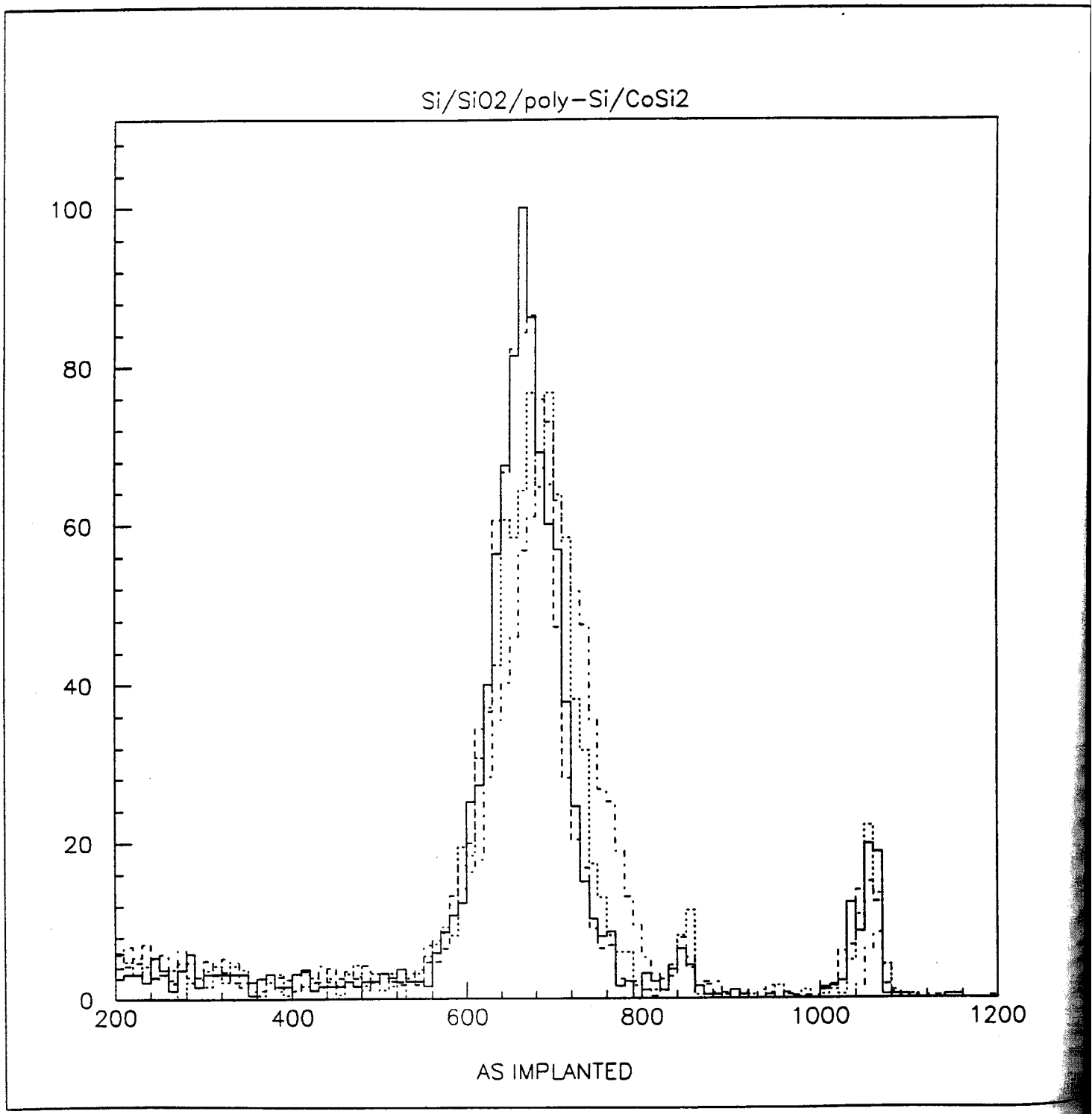
Si/SiO2/poly-Si/CoSi2
100
80
60
40
20
0
200
400
600
800
1000
1200
AS IMPLANTED

Figure 7

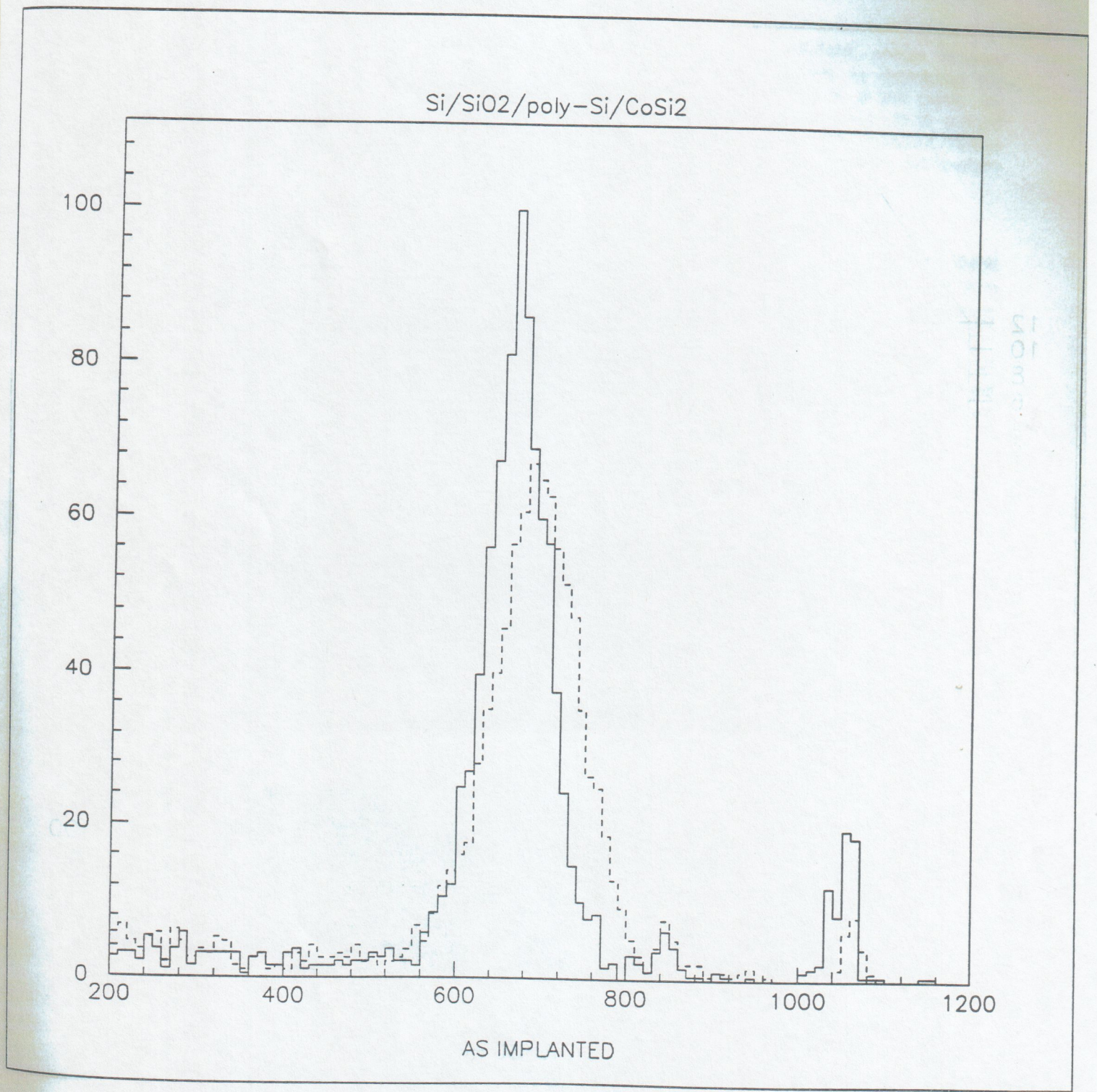
Si/SiO2/poly-Si/CoSi2
100
80
60
40
20
0
200
400
600
800
1000
1200
AS IMPLANTED

Figure 8

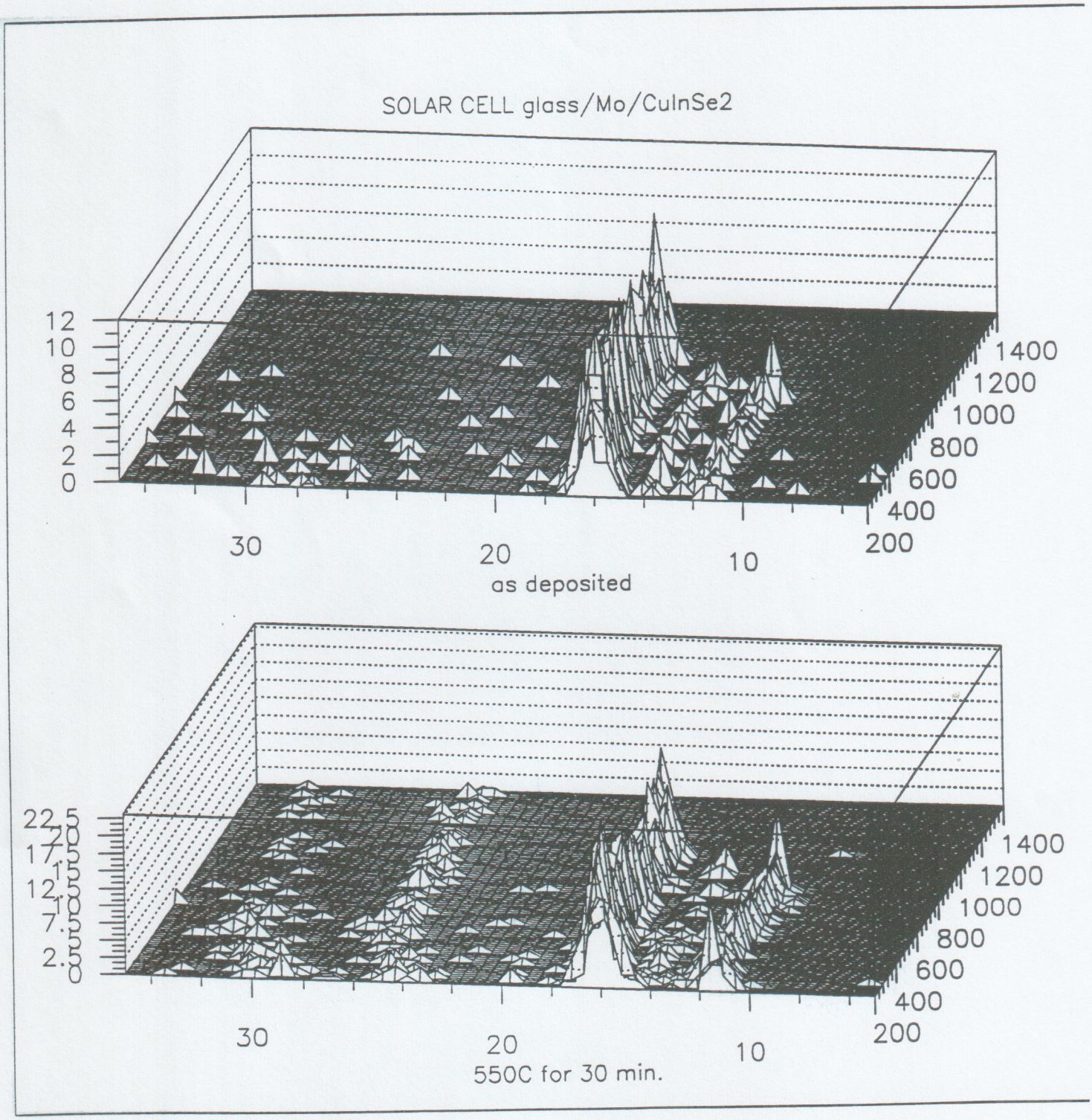
SOLAR CELL glass/Mo/CuInSe2
12
10
8
6
4
2
0
30
20
10
1400
1200
1000
800
600
400
200
as deposited
22.5
17.5
12.5
7.5
2.5
0
30
20
10
1400
1200
1000
800
600
400
200
550C for 30 min.

Figure 9